

Au+Au Collisions at RHIC and implications for ultra-relativistic astrophysical *A+A* collisions

Jens Sören Lange ^{a *}

^a Johann Wolfgang Goethe-Universität Frankfurt am Main, Institut für Kernphysik

Presented at the XIII International Symposium on Very High Energy Cosmic Ray Interactions
Pylos, Greece, 09/6-12/2004

Results from ultra-relativistic *Au+Au* collisions at RHIC are reviewed. Emphasis is put upon (a) measured properties of a *Au+Au* collision, which might be used as input to cosmic air shower Monte-Carlo event generators, (b) production of anti-matter, and (c) forward physics.

1. RHIC

The Relativistic Heavy Ion Collider (RHIC) at Brookhaven National Laboratory, New York, USA, has a circumference of 3833 m and uses 1740 superconducting magnets [1]. Fig. 1 shows the RHIC accelerator complex. The main objective of RHIC is the investigation of novel QCD phenomena at high density and high temperature in ultra-relativistic *Au+Au* collisions. The highest center-of-mass energy² $\sqrt{s}=200$ GeV is a factor $\simeq 10$ higher than past fixed target nucleus-nucleus collision experiments (e.g. CERN SPS $E_{beam}=160$ GeV, equivalent to $\sqrt{s}\simeq 17.3$ GeV). With a cross section of $\sigma_{Au+Au}=7.04$ barn (see Tab. 2), the design luminosity of $\mathcal{L}=2\cdot 10^{26}$ cm⁻²s⁻¹ means an interaction rate of $\simeq 1.4$ kHz. Four experiments are located at RHIC interaction points, i.e. the STAR, PHENIX, PHOBOS and BRAHMS experiments. The STAR experiment consists of

- a large scale midrapidity ($|\eta|\leq 1.6$) Time Projection Chamber (TPC, $R=2$ m, $L=4$ m) with $\simeq 48,000,000$ pixels (momentum resolution $\Delta p_T/p_T=3\%$ at $p_T=1$ GeV/c in a solenoidal magnetic field of $B=0.5$ T) [2]
- 2400 lead-scintillator electromagnetic calorimeter modules ($|\eta|\leq 1.0$), and
- a 3-layer silicon drift detector with $\simeq 13,000,000$ pixels ($|\eta|\leq 1.0$)

*Current Address: GSI, Planckstraße 1, 64291 Darmstadt, Germany, Email <soeren@bnl.gov>

²Throughout this paper, \sqrt{s} denotes the center-of-mass energy in the nucleon-nucleon system $\sqrt{s_{NN}}$.

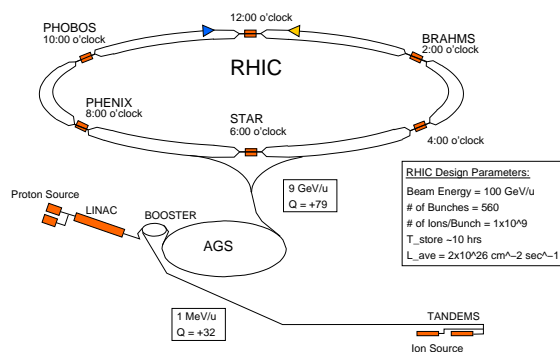


Figure 1. The RHIC accelerator complex.

The PHENIX experiment [3] consists of

- a midrapidity ($|\eta|=\pm 0.35$) electron and hadron detection system, using a ring imaging Cerenkov detector, a time-of-flight system, drift chambers (mass resolution $\Delta m/m=0.4\%$ at $m=1$ GeV) and 24,768 lead-scintillator electromagnetic calorimeter modules, and
- forward/backward ($1.1\leq |\eta|\leq 2.2$) muon chambers.

The PHOBOS experiment [4] uses 135,168 silicon strip and silicon pad readout channels in a coverage of $|\eta|=\pm 5.4$, $\Delta\varphi=360^\circ$, for unidentified charged particles, and $|\eta|=\pm 2.0$, $\Delta\varphi=180^\circ\pm 20^\circ$ for identified charged particles.

The BRAHMS experiment [5] is a spectrometer with a small opening angle of $\Delta\Omega=7.3$ msr, however at an adjustable rapidity position, thus providing particle identification from $|\eta|=0$ to $|\eta|=4$. As an example for all experiments, Tab. 1 shows the number of recorded events at the STAR ex-

periment since start of RHIC operation.

Table 1
Recorded STAR data set.

	\sqrt{s}	# of Events	Year
$Au+Au$	130.0 GeV	0.7 Mill.	2000
$Au+Au$	200.0 GeV	3.2 Mill.	2001
$Au+Au$	19.6 GeV	$\simeq 20,000$	2001
$d+Au$	200.0 GeV	35 Mill.	2003
$Au+Au$	200.0 GeV	77.9 Mill.	2004
$Au+Au$	62.4 GeV	13.3 Mill.	2004
$p+p$	200 GeV	19.8 Mill.	2004

$Au+Au$ collisions create a system of *hot* nuclear matter, $d+Au$ collisions a system of *cold* nuclear matter. The $p+p$ data set serves as reference for $Au+Au$, but at the same time is also used for the RHIC spin program, as protons in RHIC can be polarized vertical or longitudinal.

As an illustration of the amount of data, the raw data set collected at STAR experiment in 2004 compares to $\simeq 60$ times the combined raw data set of the B meson factories BELLE and BABAR. STAR also utilizes a level-3 trigger system [6], performing full event reconstruction of a central $Au+Au$ collision within $t \leq 100$ ms. Fig. 2 shows a central $Au+Au$ collision at $\sqrt{s}=200$ GeV, recorded by the level-3 trigger system at STAR, and consisting of $\simeq 6,500$ charged particle tracks and $\simeq 130,000$ TPC clusters. The level-3 trigger was used for realtime rare probe detection, such as events with anti-Helium (described in detail in Ch. 5)

2. The RHIC $Au+Au$ Collision

There are four basic stages of an $Au+Au$ collision, which are also schematically depicted in Fig. 3.

- $t=0$ fm/c. The nuclei are Lorentz contracted in the laboratory frame (“pancake shape”). Hard parton scattering occurs (qq , qg , gg scatterings).
- $t \simeq 1$ fm/c. A hot cylinder is formed. The temperature in the cylinder exceeds 10^{12} K.
- $t \simeq 4$ fm/c. Soft partons, thermally produced, emerge from the center of the collision. Beam remnant particles are peaked in the forward and backward directions.
- $t \simeq 10$ fm/c. Hadronic freeze-out occurs. All

partons confine into particles.

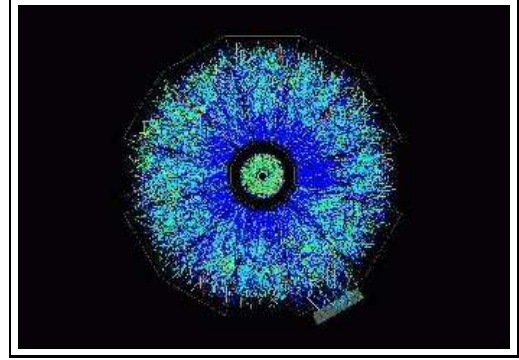


Figure 2. RHIC $Au+Au$ collision at $\sqrt{s}=200$ GeV, recorded at the STAR experiment.

Table 2
Measured parameters of a RHIC $Au+Au$ collision. For details see Ch. 2

		\sqrt{s}	Ref.
σ_{Au+Au}	(7.05 ± 0.05) barn	130	[7]
N_{part}	352 ± 3	200	[8]
N_{bin}	1051 ± 72	200	[8]
R_{out}	$(5.39 \pm 0.18 \pm 0.28)$ fm	130	[9]
R_{long}	$(5.99 \pm 0.19 \pm 0.36)$ fm	130	[9]
R_{side}	$(5.48 \pm 0.15 \pm 0.30)$ fm	130	[9]
E_T	(620 ± 33) GeV	200	[8]
E_T^{em}	(216 ± 14) GeV	200	[8]
β	$0.56c$	130	[10]
T_{chem}	(181 ± 8) MeV	130	[10]
T_{kin}	(89 ± 10) MeV	200	[11]
μ_b/T	0.18 ± 0.03	130	[12]
\bar{p}/p ratio	$0.71 \pm 0.002 \pm 0.05$	130	[13]
$\varepsilon_{Bjorken}$	(4.2 ± 0.3) GeV/fm ³	130	[14]

Tab. 2 lists the measured parameters of a RHIC collision. σ_{Au+Au} denotes the total cross section. N_{part} denotes the number of participant nucleons. N_{bin} denotes the number of binary nucleon-nucleon collisions. The size of the system can be concluded from the radii R_{out} , R_{long} and R_{side} , which are measured by quantum-mechanical Hanbury-Brown-Twiss (HBT) interferometry of $\pi^\pm \pi^\pm$ pairs, close in phase space. R_{out} denotes the radius perpendicular to the

beam axis, R_{long} parallel to the beam axis. R_{side} denotes a radius perpendicular to R_{out} , but not necessarily measured from the origin (0,0,0). R_{out} can be interpreted as the size of the particle wave front, while freezing out. In particular, the ratio $R_{out}/R_{side} \simeq 1$ indicates that RHIC freeze-out has a surprisingly short duration, an evidence which is supported by the measured high expansion velocity, given as the fraction of the speed of light $\beta=0.56$.

E_T denotes the total transverse energy, defined as the sum of the electromagnetic transverse energy E_T^{em} (i.e. leptons and photons) and the hadronic transverse energy E_T^{had} . The ratio E_T^{em}/E_T was determined to be 0.348 ± 0.019 [8]. So far, there is no indication for Centauro type events with an anomalous ratio $E_T^{em}/E_T^{had} \simeq 1/6$ [15].

The \bar{p}/p ratio visualizes how many baryons from the beam projectiles remain in the collision zone. A complete baryon-free zone would lead to a \bar{p}/p ratio $\simeq 1$, i.e. all baryons and anti-baryons are created by pair production. The measured \bar{p}/p ratio of 0.71 indicates that a significant excess of baryons over anti-baryons is still present at RHIC. As a comparison, the measured ratio is much higher than $0.00025 \pm 10\%$ at the AGS ($\sqrt{s} \simeq 4.9$ GeV) and $0.07 \pm 10\%$ at the SPS ($\sqrt{s} \simeq 17.3$ GeV), i.e. RHIC collisions represent for the first time an opportunity to advance into the almost baryon free regime.

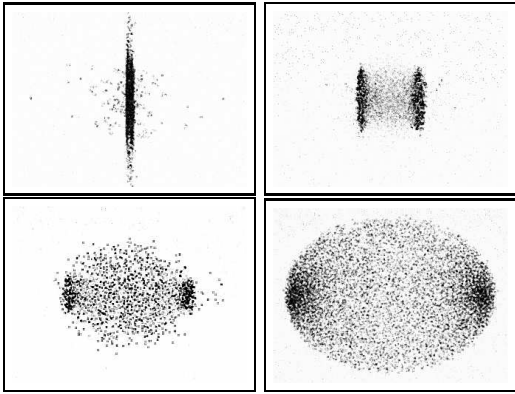


Figure 3. The four basic stages of an ultra-relativistic $Au+Au$ collision. For details see Ch. 2.

The baryo-chemical potential μ_B denotes the

energy which is necessary to add one nucleon to the system. Recent lattice QCD calculations indicate the position of the tri-critical point of strongly interacting matter at a temperature $T=(160 \pm 3.5)$ MeV and a baryo-chemical potential of $\mu_b=(725 \pm 35)$ MeV [16]. Thus, the primordial conditions in a RHIC collision are close to the critical temperature, but the baryo-chemical potential has a difference of a few hundred MeV to the tri-critical point³. As one consequence, large scale event-by-event fluctuations in the number of charged hadrons (as one might expect close to the tri-critical point) are not expected at RHIC. However, it should be noted, that in the 2-dimensional QCD phase diagram (T vs. μ_b) the primordial conditions of a RHIC collision are very close to those of the primordial universe.

2.1. The Temperature

One distinguishes between the chemical freeze-out temperature T_{chem} and the kinetic freeze-out temperature T_{kin} , which correspond to different times in the system evolution. $t(T_{chem})$ denotes the end of the *inelastic* collisions inside the particle wave front, i.e. relative particle abundances become fixed. $t(T_{kin})$ denotes the end of the *elastic* collisions and is $\simeq 100$ MeV cooler than T_{chem} . The temperature $T_{chem}=181$ MeV corresponds to $2.1 \cdot 10^{12}$ K, which can be compared to the temperature in other systems (Tab. 3). The temperature resembles one of the highest temperatures in the universe.

Also an interesting fact from the comparison of the temperatures at $\sqrt{s}=130$ GeV and $\sqrt{s}=200$ GeV shall be noted: although the collision energy increases by $\Delta E=70$ GeV, the temperature only increases by $\Delta T=7$ MeV, which corresponds to a small fraction of $\leq 10^{-6} A \cdot \Delta E$.

³Note that the new GSI accelerator facility FAIR (see Ch. 6) will test a (μ_b, T) region in the vicinity of the predicted tri-critical point, where event-by-event fluctuations might occur.

Table 3
Comparison of temperatures in various systems.

$1.4 \cdot 10^{34}$ K	Planck temperature
$2.1 \cdot 10^{12}$ K	$Au+Au$ collision
$\simeq 10^{11}$ K	mini black hole ($R=1$ fm, $M=10^{12}$ kg)
$\simeq 10^9$ K	supernova
$15 \cdot 10^6$ K	sun (core)
$55 \cdot 10^6$ K	plasma fusion
$4 \cdot 10^6$ K	laser fusion
$3 \cdot 10^4$ K	thunderstorm flash

2.2. The Matter Density

The spatial matter density, i.e. the number of partons per volume $\rho = N_{partons}/V$ can be estimated by a Bjorken ansatz [17]. If assuming that initial and final entropy are equal, the number of partons at $t \leq 1$ fm/c is equal to the measured number of final state hadrons N_{hadron} . The volume can be calculated by inserting the fireball radius (R_{out} and R_{long} in Tab. 2) into a cylindrical volume (due to Lorentz boost in the beam direction), i.e. $\rho \simeq dN_{parton}/dy \cdot 1/(\pi R^2 t)$ using the rapidity⁴ y . For a time early in the system evolution $t=0.2$ fm/c the matter density is $\rho \simeq 20/\text{fm}^3$, which corresponds to $\simeq 15 \times \rho_o$, ρ_o denoting the density of cold gold nuclei. At this high density, hadrons are definitely non-existent. In Tab. 4, the density is compared to other systems.

Table 4
Comparison of the density in various systems.

$30 \cdot 10^{17}$ kg/cm ³	$Au+Au$ collision
$2 \cdot 10^{17}$ kg/cm ³	Au nuclear density
$\sim 20,000$ kg/cm ³	Au atomic density (solid)
~ 1000 kg/cm ³	metallic hydrogen (core of planet Jupiter)
$1.1 \cdot 10^{-26}$ kg/cm ³	universe critical density

2.3. The Energy Density

About 90% of all emerging particle are π mesons, thus one may assume (as an educated guess) the π meson mass in the particle energy $E^2 = m^2 + p^2$. By (a) counting the number of charged parti-

⁴The rapidity y of a particle is defined as $y = 1/2 \cdot \ln((E+p_z)/(E-p_z))$ with the total particle energy E and the momentum component in beam direction p_z . The yield dN/dy is Lorentz invariant.

cles, (b) measuring the average particle momentum p and (c) using the volume according to Ch. 2.2, one can estimate the total energy density as $\varepsilon \simeq 5$ GeV/fm³, corresponding to a factor $\simeq 30$ higher energy density then in cold Au nuclei. For comparison, the estimate for the AGS is $\varepsilon = 1.2$ GeV/fm³, for the SPS $\varepsilon = 2.4$ GeV/fm³ [18]. A better estimate based upon perturbative QCD can be found elsewhere [7], leading to an even higher energy density of $\varepsilon \simeq 18$ GeV/fm³.

3. From $p+p$ to $Au+Au$

As RHIC experiments measure both $Au+Au$ and $p+p$ collisions in the same detector, corresponding data of both collision types can be directly compared with identical systematic errors. Fig. 4 shows transverse momentum distributions for π^- , K^- and \bar{p} for $\sqrt{s}=200$ GeV $p+p$ (top) and $Au+Au$ (bottom) as a compilation of all four RHIC experiments. One can immediately see that a $Au+Au$ collision is not a simple superposition of many $p+p$ collisions. In fact, the average mean transverse momentum $\langle p_T \rangle$ is $\simeq 390$ MeV/c for $p+p$ and $\simeq 508$ MeV/c for central $Au+Au$. The increase by $\simeq 30\%$ indicates the presence of collective effects. For further details see [19] [20].

4. Qualitative comparison to the primordial universe

A RHIC $Au+Au$ collision is sometimes being referred to as the “little bang”, in reference to the “big bang” of the primordial universe. However, a few important differences shall be noted:

- The primordial universe underwent a matter-dominated and a radiation-dominated period. At RHIC, matter dominates exclusively.
- At the time when the universe reached RHIC temperatures of $T \simeq 100$ MeV, it already had developed a macroscopical horizon distance of $L \simeq 10$ km, and thus had a size which was roughly larger than the size of a RHIC collision by a factor 10^{18} .
- The expansion velocity of $v=0.56c$ at RHIC indicates an almost explosive character. In case of the primordial universe (after inflation) it was much slower by a factor $1/M_{Planck} \simeq 10^{19}$.

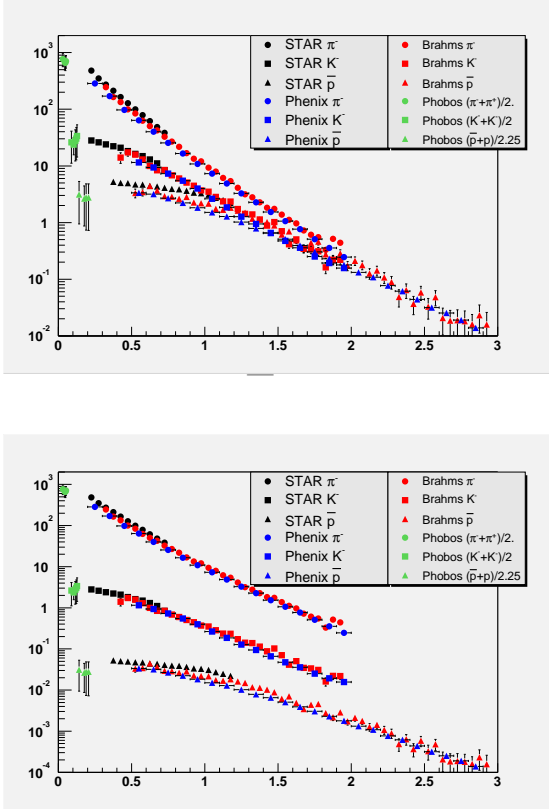


Figure 4. Transverse momentum distribution for π^- , K^- and \bar{p} for $\sqrt{s}=200$ GeV $p+p$ (top) and $Au+Au$ (bottom). For details see Ch. 3.

- In the system evolution of the universe, RHIC matter density of $\rho \simeq 15\rho_o$ occurred only for a very short period *during* inflation (assuming inflation from $10^{+118}\rho_o$ at $t \sim 10^{-36}$ s to $10^{-19}\rho_o$ at $t \sim 10^{-34}$ s). Additional details are given elsewhere [21].

5. Anti-Helium

Currently one of the most interesting questions of cosmology is: *where is the primordial anti-matter*? Several experiments (e.g. the balloon bound BESS experiment [22] at a height of $H=27$ km and the space-shuttle bound AMS experiment [23] at an orbit of $H=320-390$ km) search for direct evidence of anti-matter in cosmic rays. It should be noted that incident particle energies at the AMS orbit location (i.e. quasi-

“beam” energies) range from 10^1-10^6 MeV per nucleon, comparable to RHIC beam energies at 10^5 MeV per nucleon. A particularly suited probe for anti-matter search is anti- He , as the signature of charge $Z=-2$ is clean⁵. A $Z=-1$ signature of \bar{p} is contaminated by K^- and π^- mesons. The STAR level-3 trigger system was used to identify $Z=-2$ candidate events in realtime. Primordial Helium is not rare, but in fact represents $\simeq 24\%$ of all primordially created matter (created at time scales $t \sim 1$ s and at temperatures $T \sim 0.1$ MeV). Under the assumption of an *a priori* symmetric primordial production of He and anti- He , one may conclude that anti- He might be detectable, too.

In a RHIC $Au+Au$ collision, there is trivially no anti-matter in the initial state, as nuclei are completely made of matter. However, even anti-nuclei are created in a detectable quantity. The dominant anti-nuclei production mechanism is a two-step process, namely (1) pair production of $p\bar{p}$, $n\bar{n}$, followed by (2) coalescence, i.e. the anti-nucleon wave functions overlap inside a homogeneity volume. For the systematic study of the A dependence of anti-nuclei production yields, it is useful to define an *invariant yield*

$$E \frac{d^3 N_A}{d^3 P} = B_A (E \frac{d^3 N_N}{d^3 p})^A \quad (1)$$

with anti-nuclei yield N_A , the anti-nucleon yield N_N , the anti-nucleon momentum p , and $p=P/A$. The coalescence coefficient B_A denotes the probability that A anti-nucleons form a bound state. It might be regarded as a “penalty factor” for the step from n to $n+1$ anti-nucleons in the system. Typical orders of magnitude are $B_2 \sim 10^{-3}$ and $B_3 \sim 10^{-6}$. For high \sqrt{s} and a large system size, the coalescence coefficient is related to the inverse of the effective volume containing the anti-nuclei (i.e. the fireball volume) by $B_A = 1/V_{eff}^{A-1}$.

So far, STAR has been able to collect a raw yield of 193 anti- 3He in a total of $4 \cdot 10^6$ $Au+Au$ events at $\sqrt{s}=200$ GeV. In the same data set, 6416 anti-deuterons were also identified and used for a de-

⁵Except anti- He and hypothetical pentaquark states there are no other stable $Z=-2$ particles predicted in nature.

termination of B_2 . Further details are given elsewhere [24]. Fig. 5 shows the measured ionization dE/dx vs. momentum for the anti- He candidates in the STAR Time Projection Chamber.

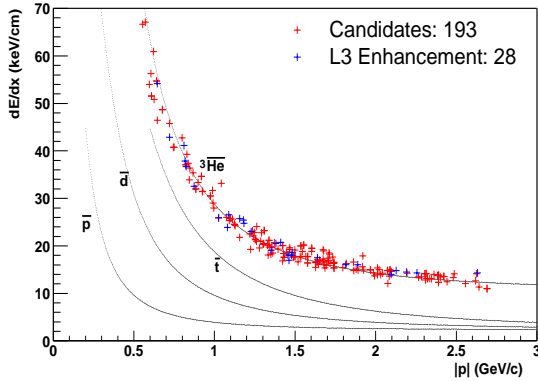


Figure 5. Ionization dE/dx vs. momentum p for anti- He in the STAR Time Projection Chamber (blue : level-3 trigger, red : offline analysis).

Fig. 6 shows the extracted coalescence coefficient B_3 in comparison to other measurements. RHIC represents the highest energy ever at which anti- He was created in a accelerator experiment.

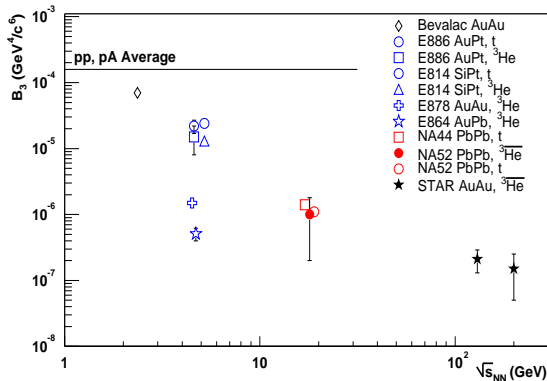


Figure 6. Coalescence coefficient B_3 for anti- 3He and anti- t production vs. \sqrt{s} for different experiments.

As an important result, the coalescence (and thus the yield of produced anti-nuclei per one collision) in $Au+Au$ (normalized to the number of binary collisions) at RHIC is approximately a factor of 40 smaller then in $p+p$ or in $\gamma+p$ [25].

The coalescence coefficient is also an important input to calculations of anti- He yield from nucleus-nucleus collisions in the stellar medium [26], which is the dominant background for the primordial anti- He search by AMS.

The STAR 2004 data set is currently being analyzed. The data are expected to contain 2.7 ± 0.3 anti- 4He , which would be a first experimental observation.

6. Forward Physics

For high energy $p+A$ collisions in the earth's upper atmosphere, a proper knowledge of the particle shower in the forward rapidity region is very important, as the forward particles are the visible center of the showers as seen on the detector systems at sea level. Ideally $p+Au$ collisions would be preferable, but due to technical accelerator issues⁶ $d+Au$ collisions were chosen at RHIC. As shown in Tab. 1, several million $d+Au$ collisions were recorded at RHIC in 2003. Fig. 7 shows the rapidity distribution of particles from a $d+Au$ collision at $\sqrt{s}=200$ GeV with data from BRAHMS [27], in comparison to a perturbative QCD calculation [28]. The η asymmetry ratio of forward (Au side) to backward (d side) is a characteristic of the collision system. STAR measured the ratio for these collisions as a function of p_T (Fig. 8) [29]. As a surprising result, for $0 \leq |\eta| \leq 0.5$ the ratio is flat, but for $0.5 \leq |\eta| \leq 1.0$ the ratio shows a rising behaviour up to $p_T \simeq 2-3$ GeV/c, followed by a descending slope for higher p_T . Fig. 8 also shows the comparison to model calculations, including (a) shadowing⁷ and (b) saturation at high gluon densities. The data seem to support a saturation ansatz, which, in a geometrical picture, assumes that the probability that two gluons collide is one. $p+A$ collisions will also be an important part of the future GSI accelerator facility FAIR at Darmstadt, Germany (Fig. 9), which will provide p beams for fixed target experiments up to

⁶One the one hand, the d beam has a charge/mass ratio close to the Au beam. On the other hand the beam-beam interaction, which shortens the lifetime of a RHIC store, is in the case of $p+Au$ a factor of $\simeq 2$ higher than in the case of $d+Au$.

⁷Shadowing is the depletion of parton distributions at small x inside a nucleus.

90 GeV.

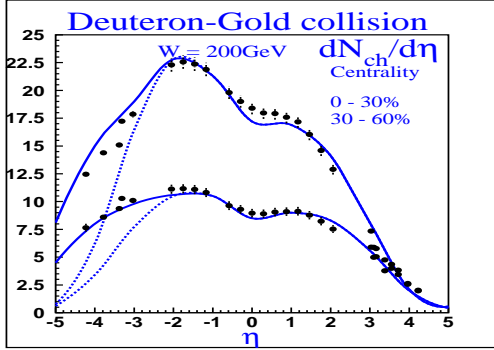


Figure 7. Pseudorapidity distribution for charged particles from $d+Au$ collisions at $\sqrt{s}=200$ GeV in BRAHMS [27] for two different centralities, corresponding to two different impact parameter ranges.

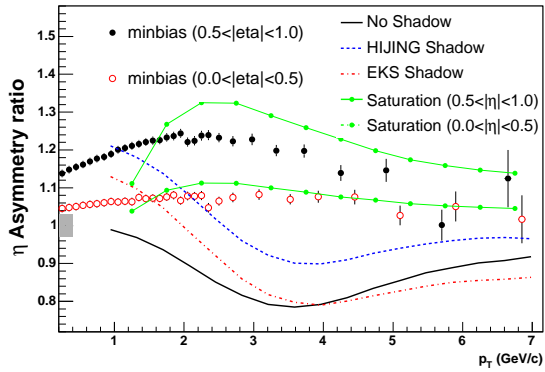


Figure 8. Forward/backward pseudorapidity ratio vs. p_T $d+Au$ collision at $\sqrt{s}=200$ GeV in STAR [29]. For details see Ch. 6.

Another important class of forward reactions are ultra-peripheral $Au+Au$ collisions, in which the Au nuclei interact by a very strong electromagnetic field (10^{20} V/cm at the surface of the nuclei). Photons produced in these strong fields are peaked forward, and may create vector mesons by scattering off the Au nuclei. Fig. 10 shows the differential cross section $d\sigma(\gamma Au \rightarrow \rho^0 Au)/dt$ vs. the momentum transfer t . The very small t values indicate the forward scattering. From an exponential fit (shown as line in Fig. 10) a forward cross section was determined to be

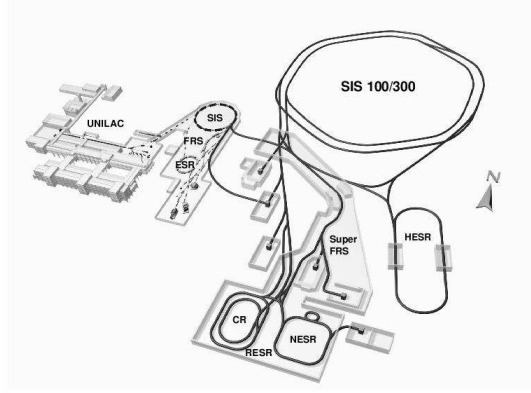


Figure 9. The future GSI accelerator complex FAIR.

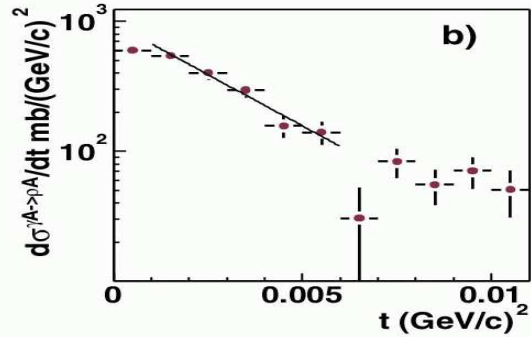


Figure 10. Forward differential cross section $d\sigma(\gamma Au \rightarrow \rho^0 Au)/dt$ vs. t [30].

$d\sigma/dt|_{t=0} = 965 \pm 140 \pm 230$ mb/GeV². Details are given elsewhere [30].

7. Charm cross sections

For high energy cosmic nuclear collisions in the galactic medium or the earth's atmosphere, the knowledge of heavy quark production cross sections is very important. Both STAR [31] and PHENIX [32] have measured the charm cross section. Fig. 11 shows the total $c\bar{c}$ cross section per nucleon-nucleon collision vs. \sqrt{s} . There is a preliminary indication that the measured cross section is higher than the expected cross section extrapolation obtained from (a) PYTHIA Monte-Carlo simulation (based upon Lund fragmentation) [33] and (b) a NLO QCD calculation [34].

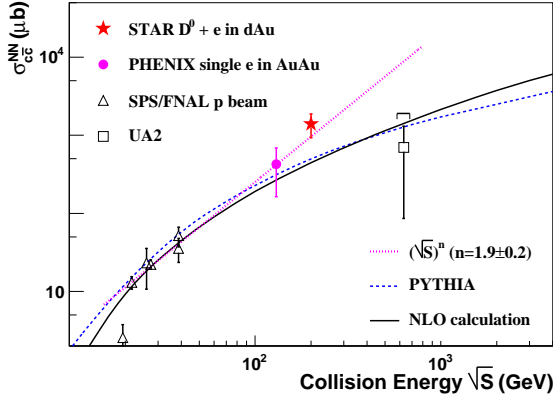


Figure 11. Total $c\bar{c}$ cross section per nucleon-nucleon collision vs. \sqrt{s} . For details see [31].

8. Summary

In 4 years of operation, RHIC has collected a data set of millions of $p+p$, $d+Au$ and $Au+Au$ collisions. From the analysis we may conclude that a RHIC $Au+Au$ collision is a very hot and very dense hadronic system, which expands explosively with $v=0.56c$. During the short freeze-out the system undergoes a graceful QCD self-organisation, which could be successfully described by models based upon perturbative QCD. One of the most basic but also most important observations is that a $Au+Au$ collisions is not a simple superposition of $p+p$ collisions, but in fact the mean transverse momentum increases by $\simeq 30\%$, indicating collective effects.

REFERENCES

1. <http://www.bnl.gov/rhic>
2. <http://www.star.bnl.gov>
3. <http://www.phenix.bnl.gov>
4. <http://www.phobos.bnl.gov>
5. <http://www.rhic.bnl.gov/brahms>
6. J. S. Lange et al., Nucl. Instr. Meth. **A499**(2003)778
7. D. Kharzeev, M. Nardi, nucl-th/0012025, Phys. Lett. **B507**(2001)121
8. The STAR Collaboration, nucl-ex/0407003
9. The STAR Collaboration, nucl-ex/0107008, Phys. Rev. Lett. **87**(2001)0C82301
10. The STAR Collaboration, nucl-ex/0307024, Phys. Rev. Lett. **92**(2004)182301
11. The STAR Collaboration, nucl-ex/0310004, Phys. Rev. Lett. **92**(2004)112301,
12. The STAR Collaboration, nucl-ex/0211024, Phys. Lett. **B567**(2003)167,
13. The STAR Collaboration, nucl-ex/0104022, Phys. Rev. Lett. **86**(2001)4778, Err. Phys. Rev. Lett. **90**(2003)119903(E)
14. The STAR Collaboration, nucl-ex/0311017
15. M. Tamada et al., Nuovo Cim. B41(1977)245
16. Z. Fodor, S. D. Katz, hep-lat/0106002, JHEP 0203(2002)014
17. J. D. Bjorken, Phys. Rev. **D27**(1983)140
18. A. Andronic, P. Braun-Munzinger, hep-ph/0402291
19. The STAR Collaboration, nucl-ex/0310004, Phys. Rev. Lett. **92**(2004)112301
20. The STAR Collaboration, nucl-ex/0211004, Nucl. Phys. **A715**(2003)399
21. J. S. Lange, hep-ph/0403104
22. The BESS Collaboration, astro-ph/9710228 Phys. Lett. **B422**(1998)319
23. The AMS Collaboration, hep-ex/0002048, Phys. Lett. **B472**(2000)215,
24. J. S. Lange, C. Struck, nucl-ex/0403008, Nucl. Phys. **A738**(2004)396
25. The H1 Collaboration, hep-ex/0403056, Eur. Phys. J. **C36**(2004)413
26. P. Chardonnet, J. Orloff, P. Salati, astro-ph/9705110, Phys. Lett. **B409**(1997)313,
27. The BRAHMS Collaboration, nucl-ex/0401025
28. D. Kharzeev, E. Levin, M. Nardi, hep-ph/0212316, Nucl. Phys. **A730**(2004)448
29. The STAR Collaboration, nucl-ex/0408016
30. The STAR Collaboration, nucl-ex/0206004, Phys. Rev. Lett. **89**(2002)272302
31. The STAR Collaboration, nucl-ex/0407006
32. The PHENIX collaboration, nucl-ex/0202002, Phys. Rev. Lett. **88**(2002)192303
33. T. Sjöstrand et al., Comp. Phys. Comm. **135**(2001)238
34. R. Vogt, hep-ph/0203151, Int. J. Mod. Phys. **E12**(2003)211